Electronic Supplementary Material (ESI) for Dalton Transactions.

Supporting Information

Aryl selenonium vs. aryl sulfonium counterions in polyoxometalate chemistry: the impact of Se^+ cationic centers on the photocatalytic reduction of dichromate

Mahender Singh, Aakash Yadav, Ranjit Singh, and Chullikkattil P. Pradeep*

*School of Chemical Sciences, Indian Institute of Technology Mandi, Mandi – 175075, Himachal Pradesh, India.

Fax: +91 1905 267 009; Tel: +91 1905 267 045; E-mail: pradeep@iitmandi.ac.in

Characterization. The organic counterion precursors methyldiphenylsulfonium trifluoromethanesulfonate (MDPST), methyldiphenylselenonium trifluoromethanesulfonate (MDPSeT) and their octamolybdate hybrids, **1** and **2**, were characterized using several analytical and spectroscopic techniques. Fourier transform infrared (FT-IR) spectroscopy analyses were performed using PerkinElmer Spectrum 2 spectrometer with KBr pellets. The powder X-ray diffraction (PXRD) analyses were performed on a Rigaku SmartLab 9 kW rotating anode diffractometer working in Bragg configuration with Ni-filtered Cu Kα irradiation (λ = 0.1542 nm) at 45 kV and 100 mA. The diffraction patterns were collected in the range of 5 – 60^o with a scan rate of 2^o per min. The electrospray ionization mass spectrometry (ESI-MS) analyses were performed using a Bruker HD compact instrument equipped with Bruker Data analysis software in negative mode. The thermal gravimetric analysis (TGA) of both hybrids was performed in an instrument NETZSCHSTA 449 F1 JUPITER in a temperature range of 25 to 700 ^{o}C with the heating rate of 10 ^{o}C min^{-1} under N_2 atmosphere. The chemical analysis of all the samples was achieved through X–ray photoelectron spectroscopy (XPS) by a Thermo Scientific NEXSA photo-emission spectrometer with Al-Kα (1486.6 eV) X-ray radiation. The XPS data were processed using Avantage software. The morphological investigations of the hybrids were performed using field emission scanning electron microscopy (FE-SEM) on an FEI Nova Nano SEM-450 instrument. The ^{1}H, ^{13}C, and ^{19}F nuclear magnetic resonance (NMR) spectra were recorded using a Jeol JNM ECX – 500 FT-NMR spectrometer. Deuterated dimethylsulfoxide (DMSO-d_6) was used as the solvent and tetramethylsilane (TMS) as an internal standard for NMR analyses. The photocatalytic experiments were performed in a homemade UV photoreactor equipped with LZC-UVA (λ_{exc} = 365 nm, P = 8 W) lamps from Luzchem. The ultraviolet–visible (UV-vis) spectroscopy analyses were performed on a Shimadzu UV-2450 spectrophotometer. The optical absorption and reflectance of the solid-state hybrids were analyzed by diffused reflectance spectroscopy (DRS) on a Perkin Elmer UV-visible-NIR Lambda 750 spectrophotometer using the diffuse reflectance standard polytetrafluoroethylene (PTFE) polymer. The PL spectra of the hybrids were recorded in the solid state using a Fluorolog-3 Spectrofluorometer (HORIBA-Jobin-Yvon).

Single Crystal X-ray Crystallography: The single-crystal XRD data was collected using an Agilent SuperNova diffractometer having Cu and Mo dual source and Eos CCD detector, using Cu K_α(λ = 1.54184Å) at 293 K. Data acquisition, reduction, and absorption correction were performed using the CrysAlisPRO program.[1] The structure solving was done with ShelXS and refined on F^2 by full-matrix least-squares techniques using the ShelXL[2] program provided in the Olex[2] (v.1.2) program package.[3] The anisotropic displacement parameters were applied for all the atoms, except hydrogen atoms. CCDC 2297062 contains the supplementary crystallographic data of MDPSeT.

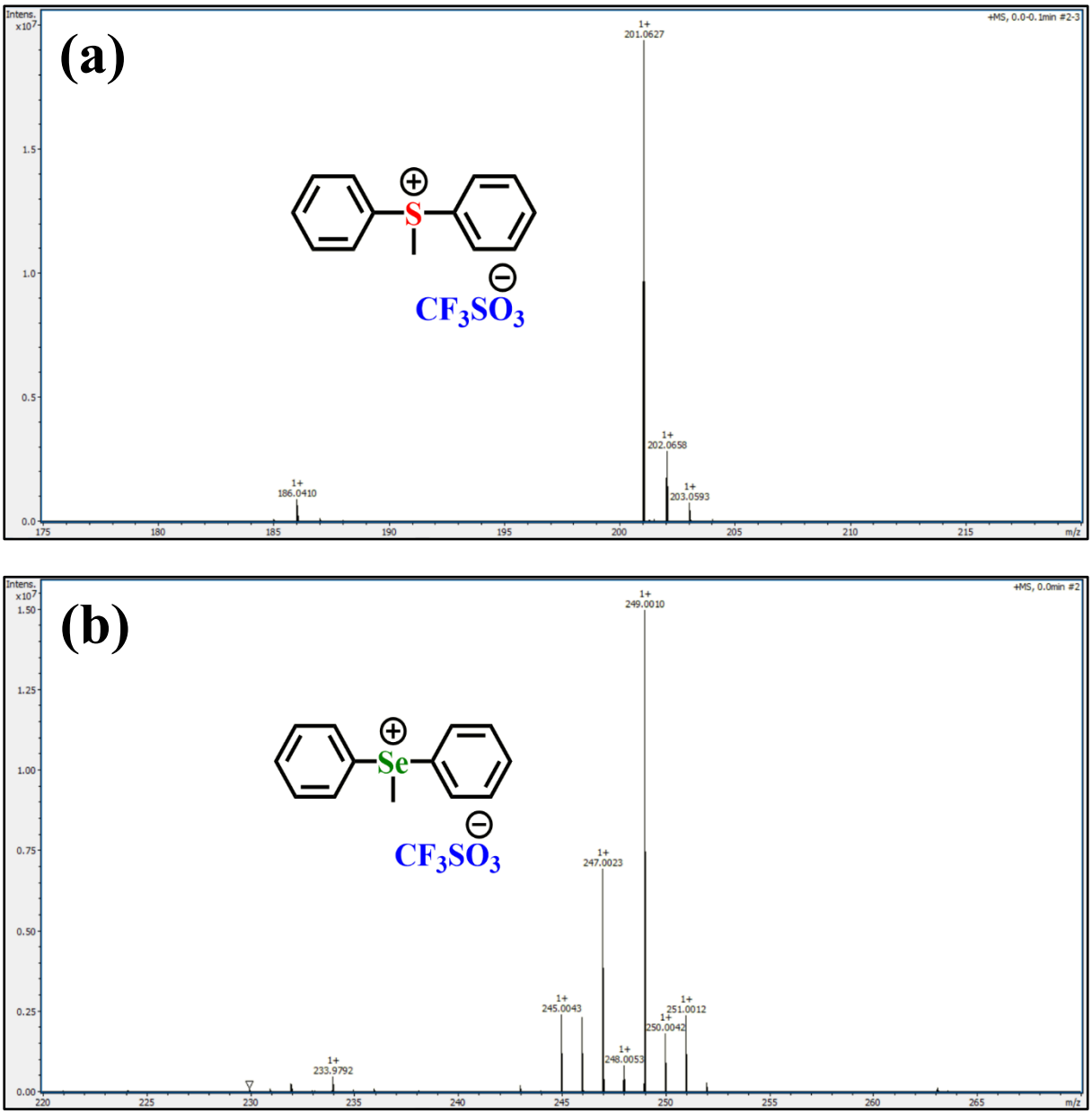

Fig. S1 (a) ESI-MS (positive mode) data of (a) MDPST; and (b) MDPSeT.

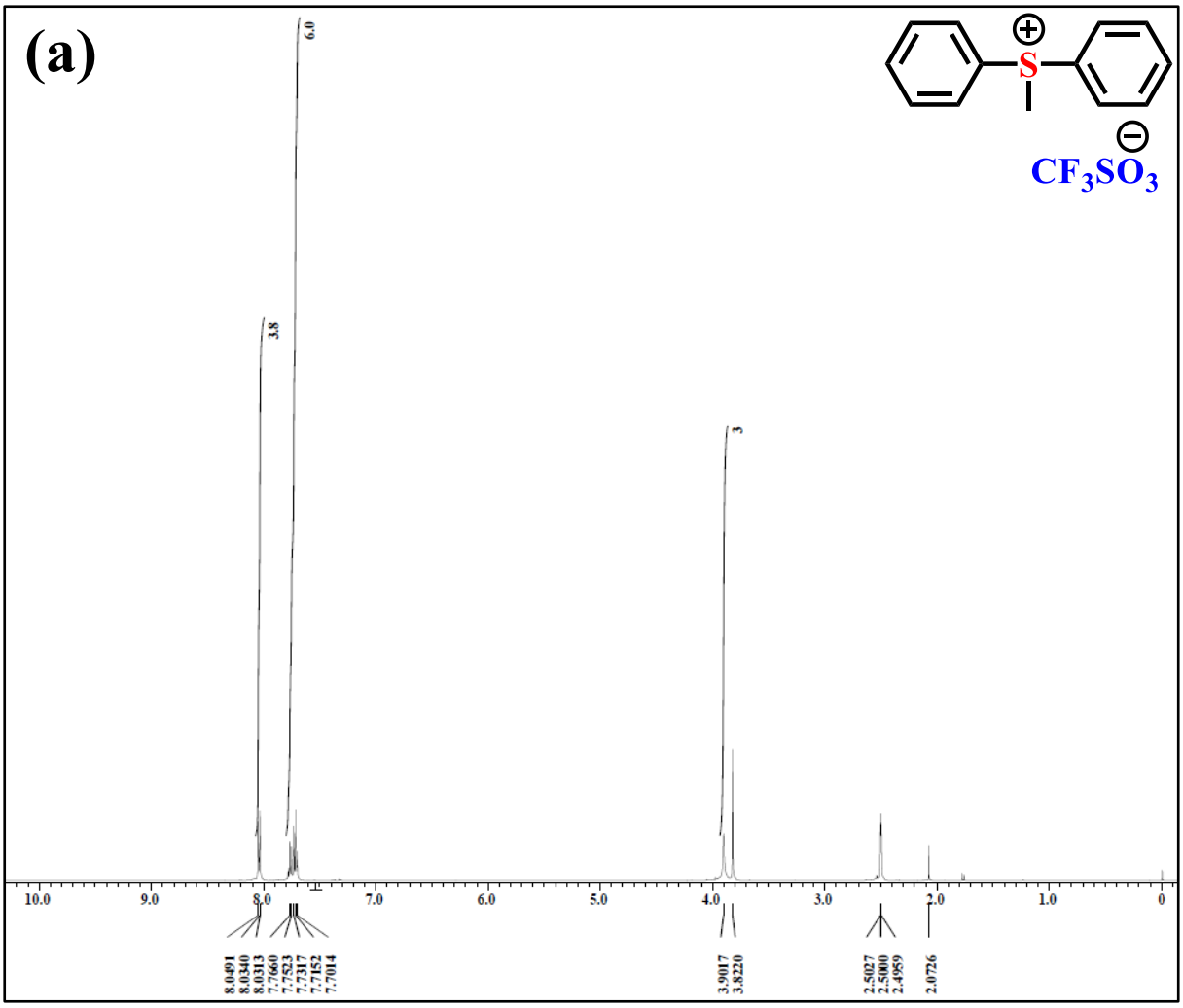

Fig. S2 (a) ^{1}H - NMR spectrum of MDPST.

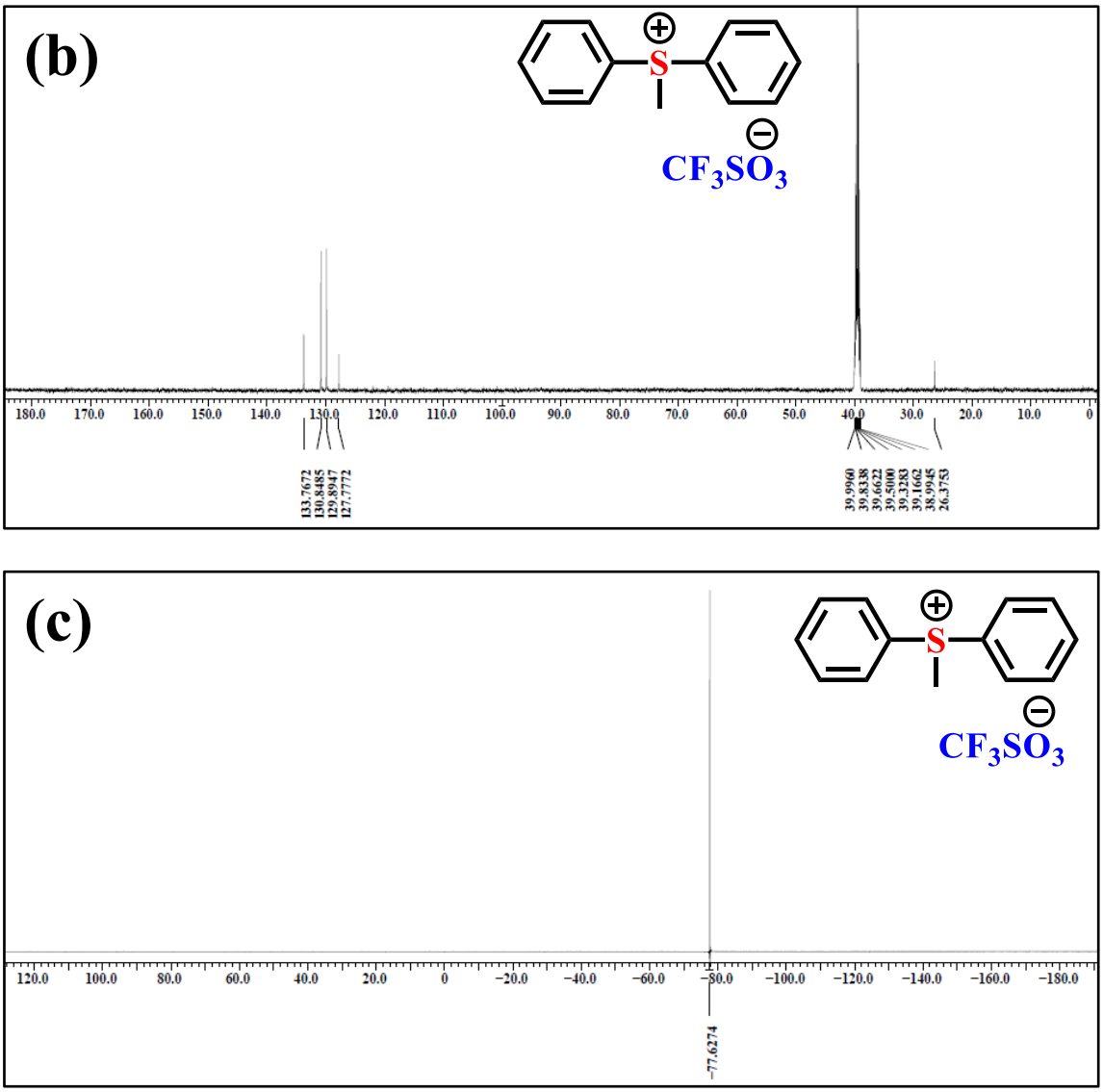

Fig. S2 (b) ^{13}C and (c) ^{19}F – NMR spectra of MDPST.

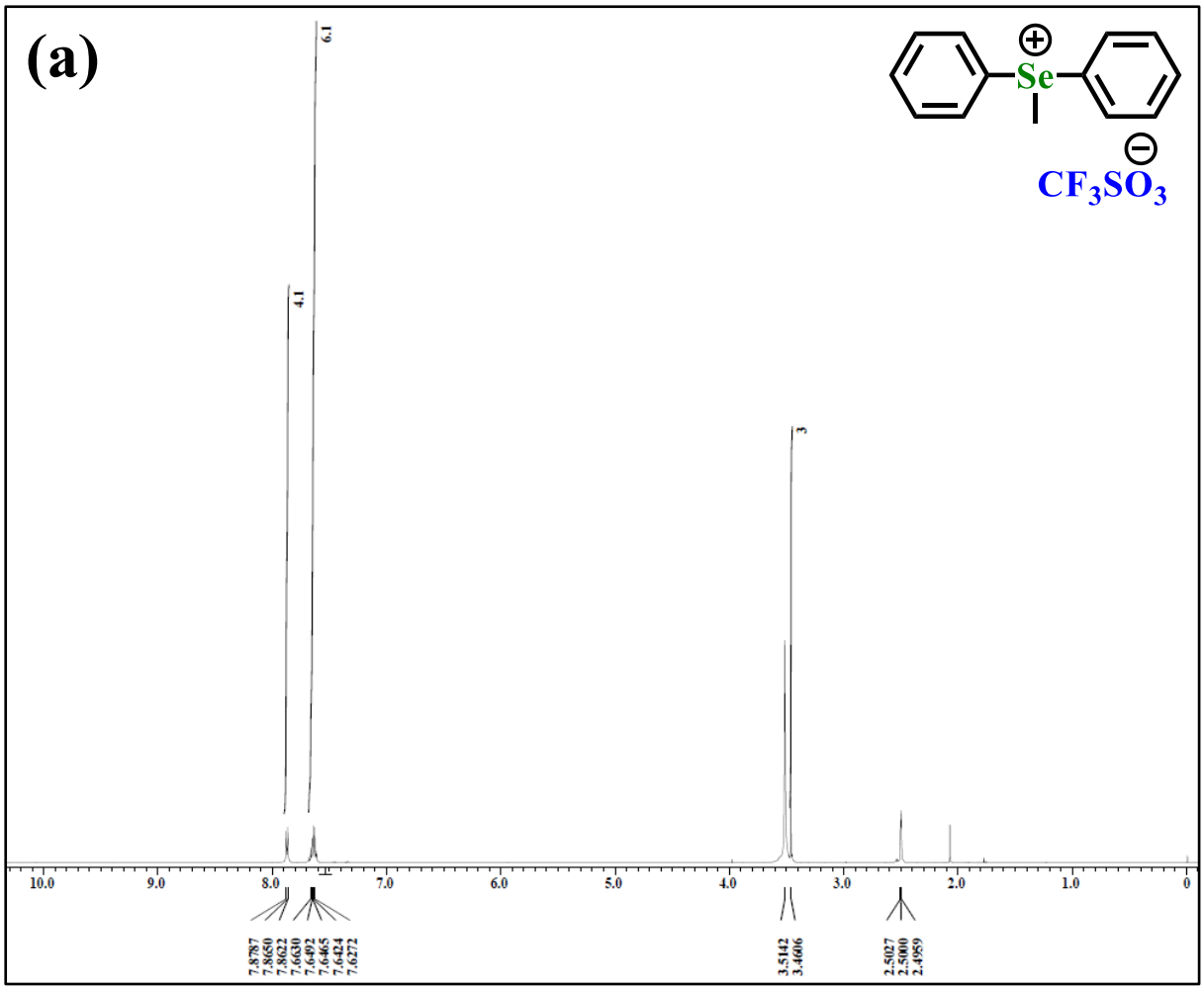

Fig. S3 (a) ^{1}H - NMR spectrum of MDPSeT.

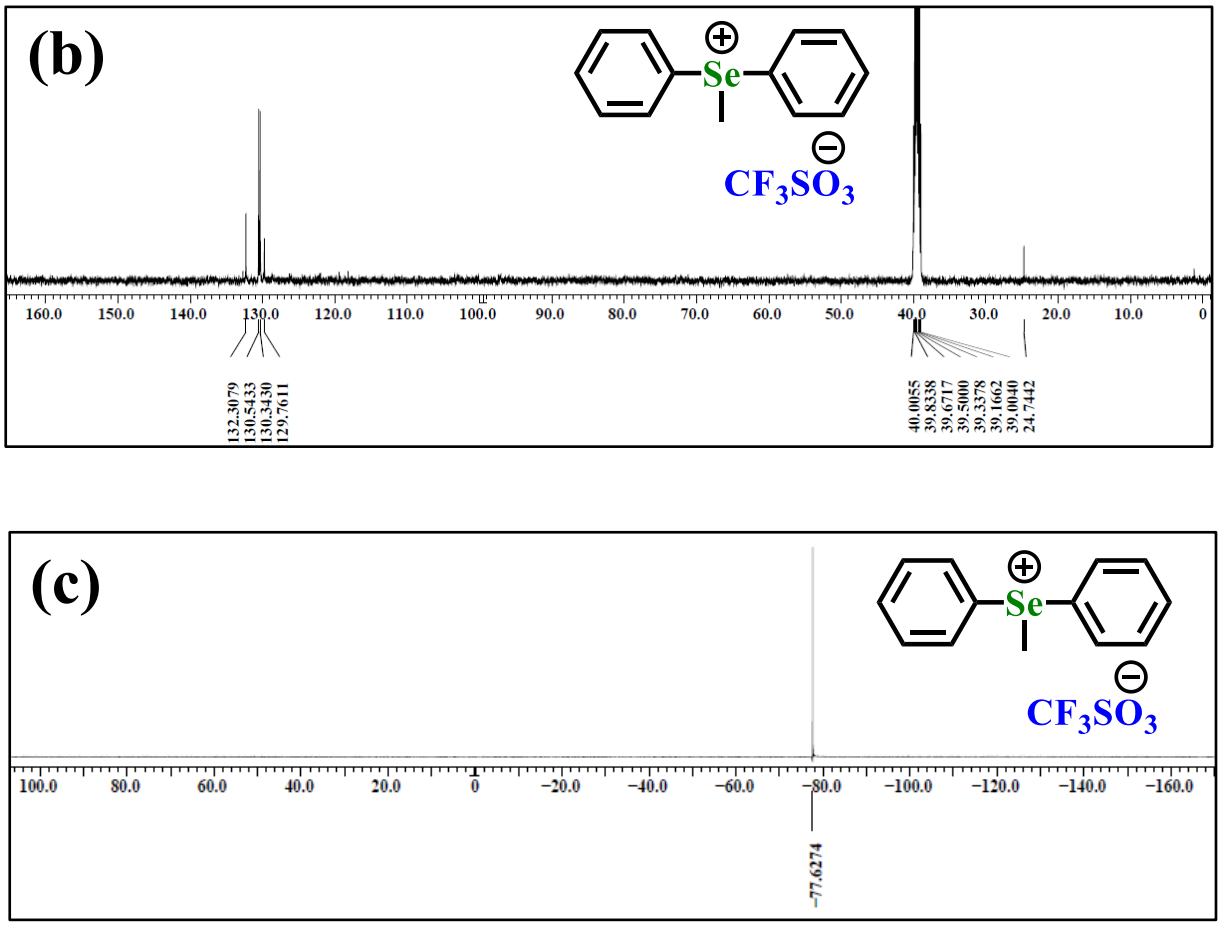

Fig. S3 (b) ^{13}C and (c) ^{19}F – NMR spectra of MDPSeT.

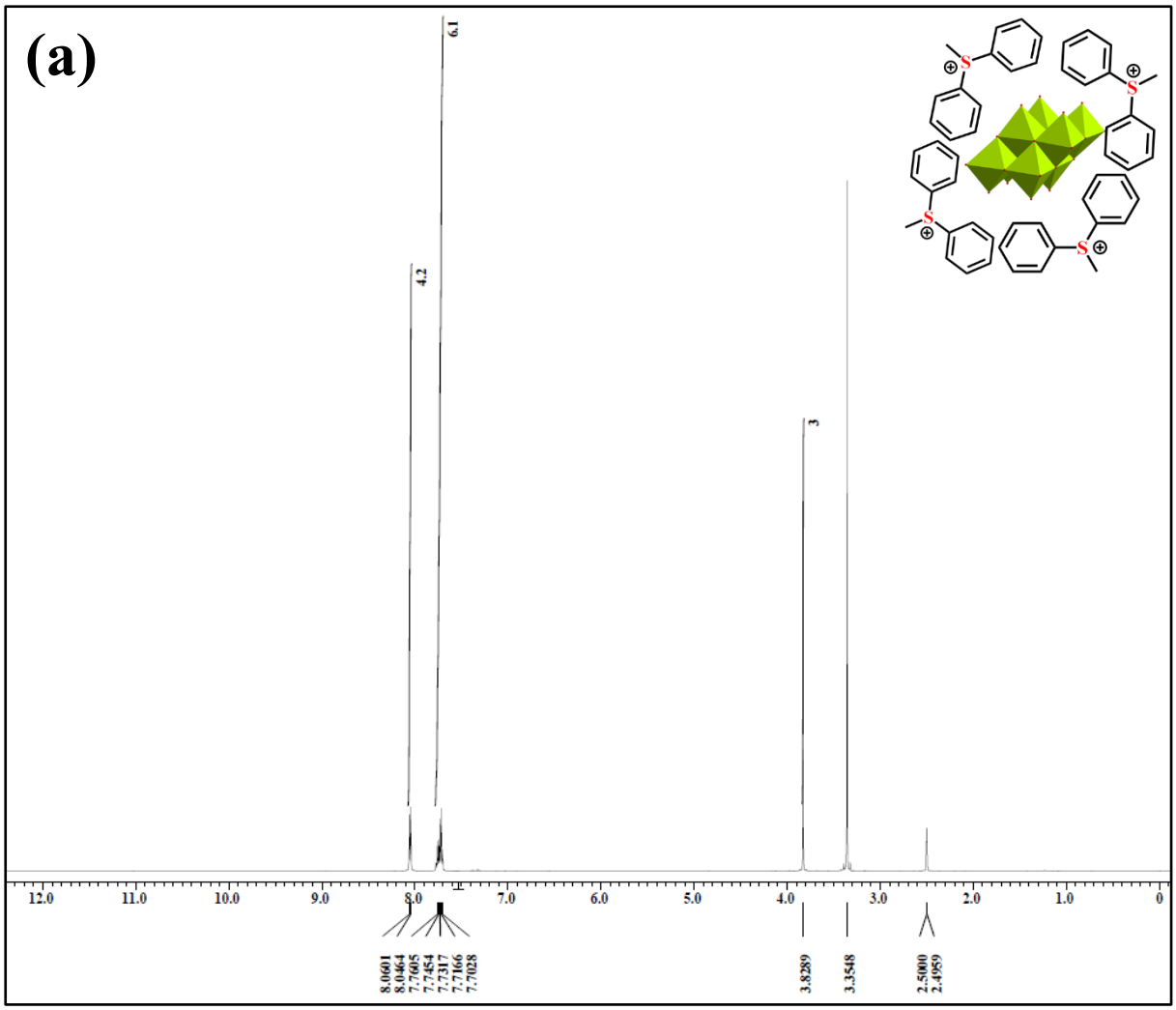

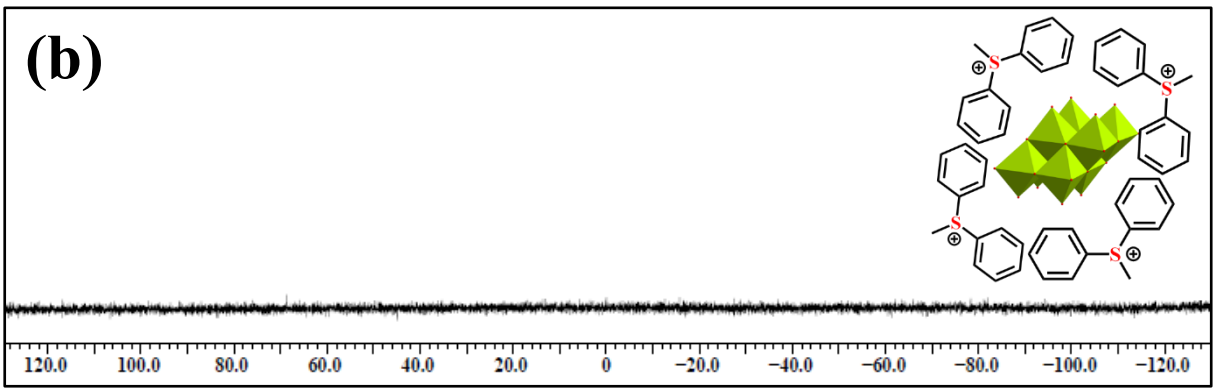

Fig. S4 (a) ^{1}H and (b) ^{19}F – NMR spectra of hybrid **1**.

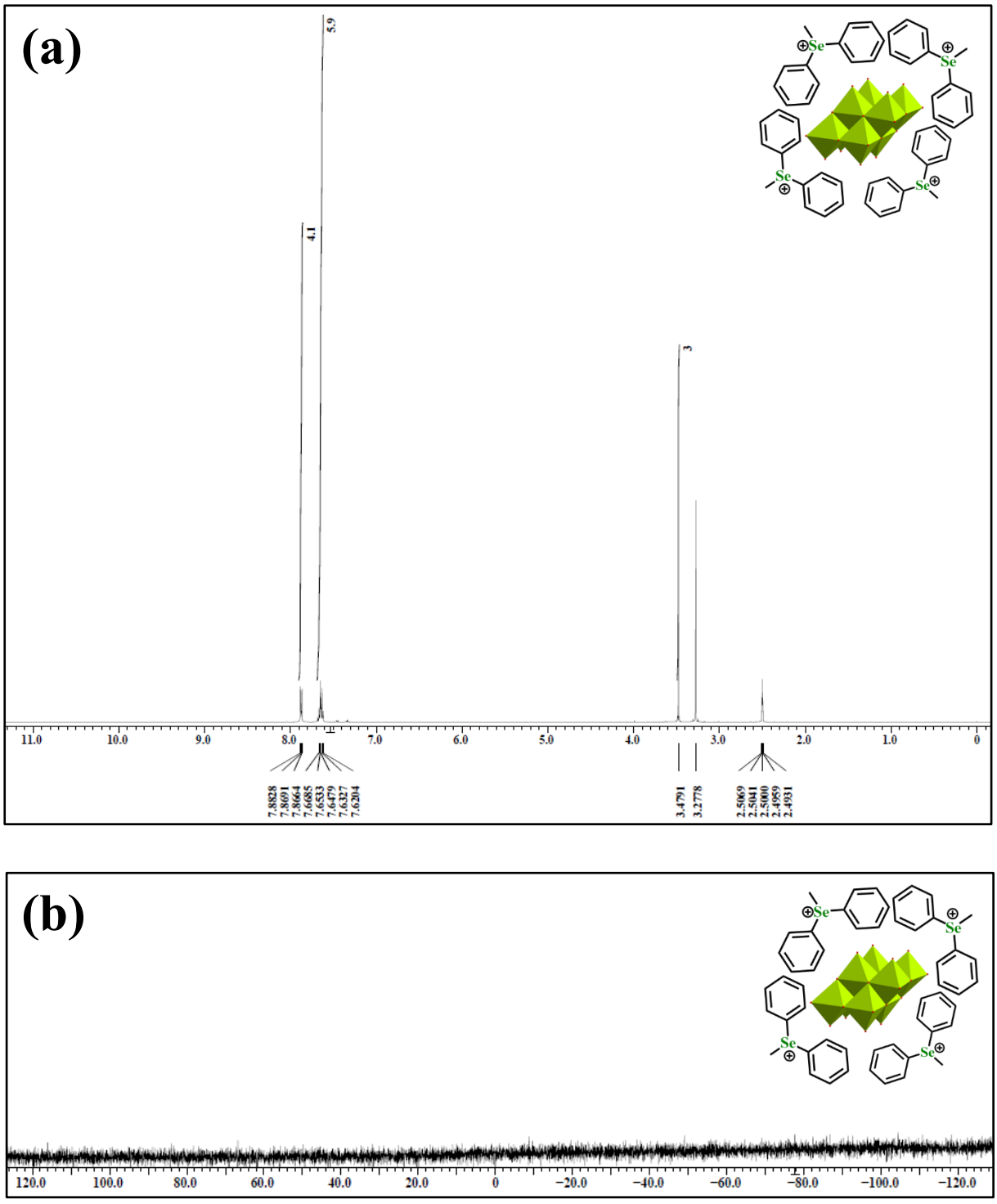

Fig. S5 (a) ^{1}H and (b) ^{19}F – NMR spectra of hybrid **2**.

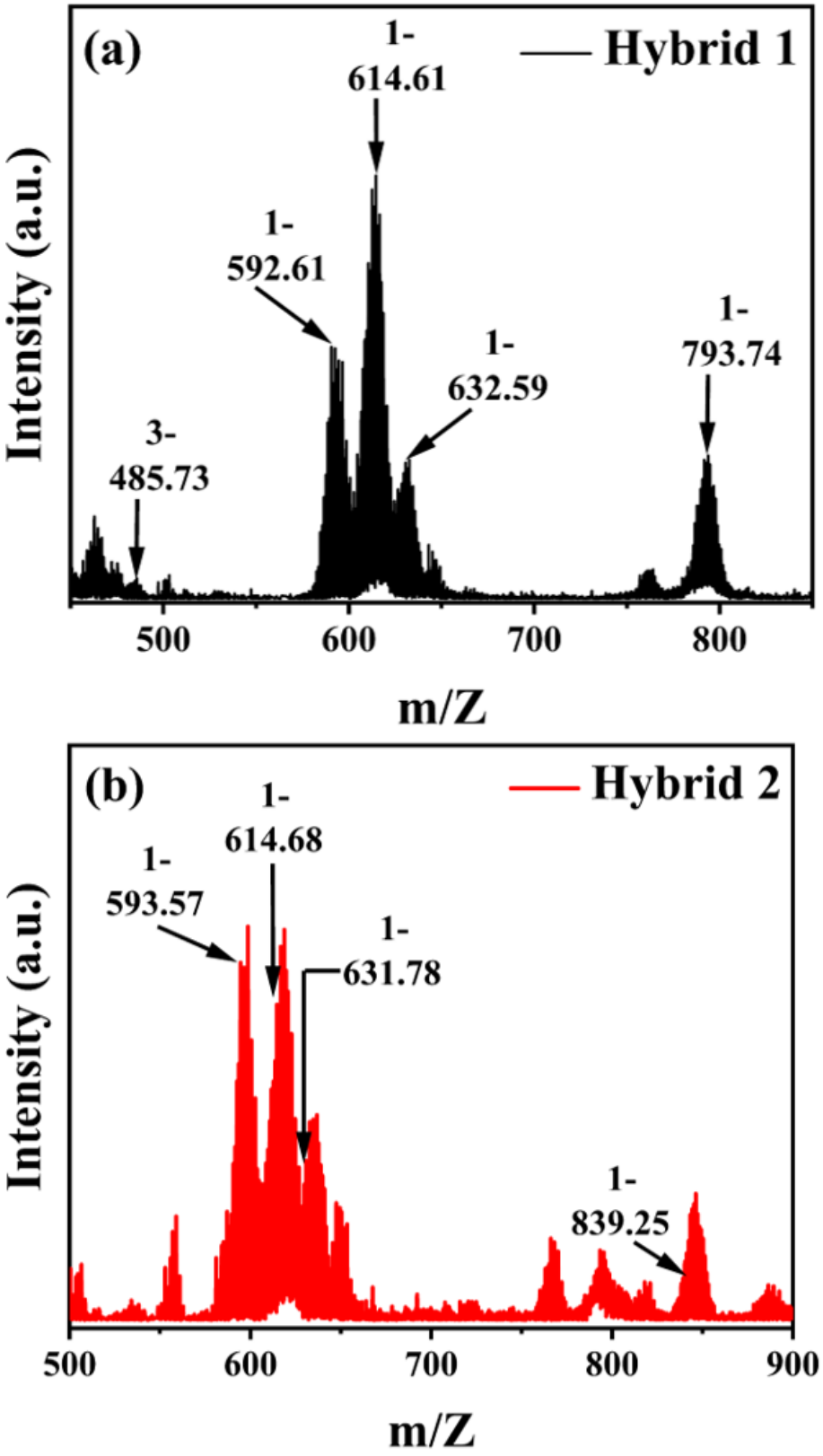

Fig. S6 ESI-MS (negative mode) data of (a) hybrid **1**; and (b) hybrid **2**.

Table S1. Detailed assignment of mass spectral data of hybrid **1**.

Sr. No.	Ion (hybrid 1)	m/Z calculated	m/Z observed
1.	$(H)[Mo_4O_{13}]^{1-}$	592.76	592.61
2.	$(Na)[Mo_4O_{13}]^{1-}$	614.74	614.61
3.	$(K)[Mo_4O_{13}]^{1-}$	630.85	632.59
4.	$(C_{13}H_{13}S)[Mo_4O_{13}]^{1-}$	793.06	793.74
5.	$(C_{13}H_{13}S)[Mo_8O_{26}]^{3-}.4H_2O$	485.62	485.73

Table S2. Detailed assignment of mass spectral data of hybrid **2**.

Sr. No.	Ion (hybrid 2)	m/Z calculated	m/Z observed
1.	$(H)[Mo_4O_{13}]^{1-}$	592.76	593.57
2.	$(Na)[Mo_4O_{13}]^{1-}$	614.74	614.68
3.	$(K)[Mo_4O_{13}]^{1-}$	630.85	631.78
4.	$(C_{13}H_{13}Se)[Mo_4O_{13}]^{1-}$	839.95	839.25

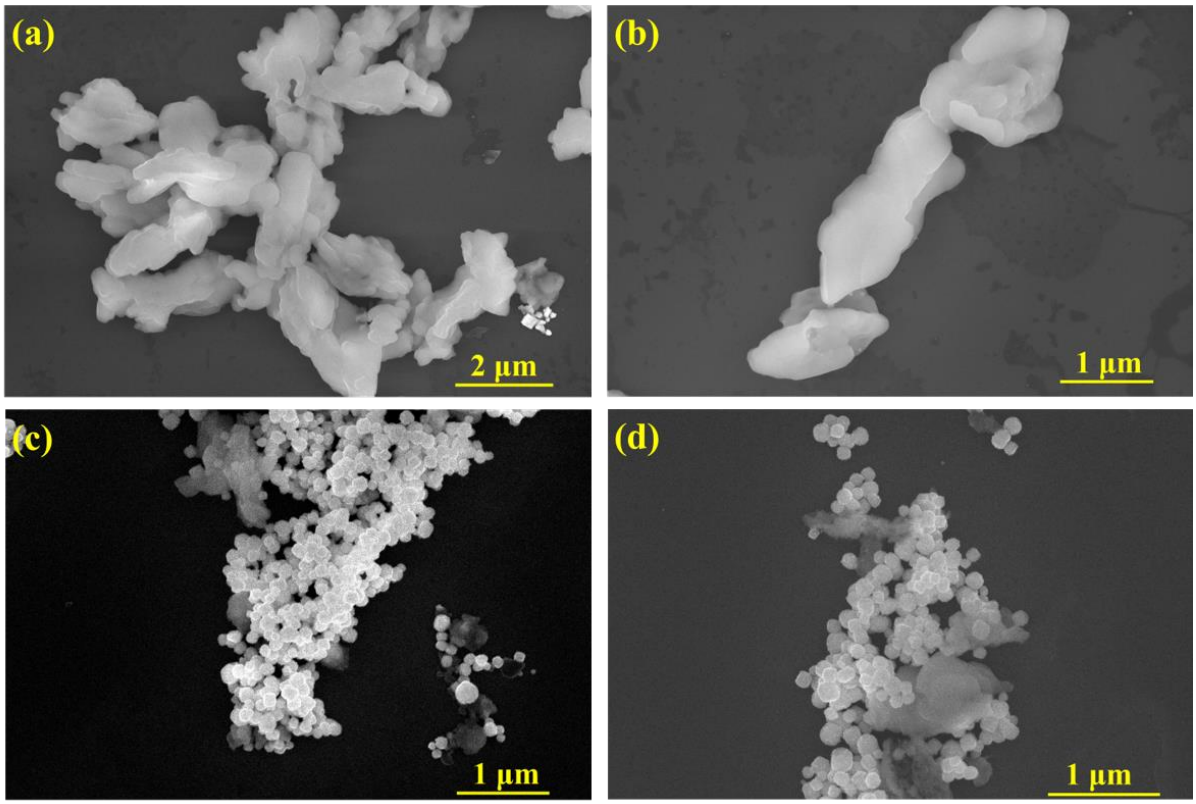

Fig. S7 FE-SEM images of hybrid **1** (a, b); and of hybrid **2** (c, d).

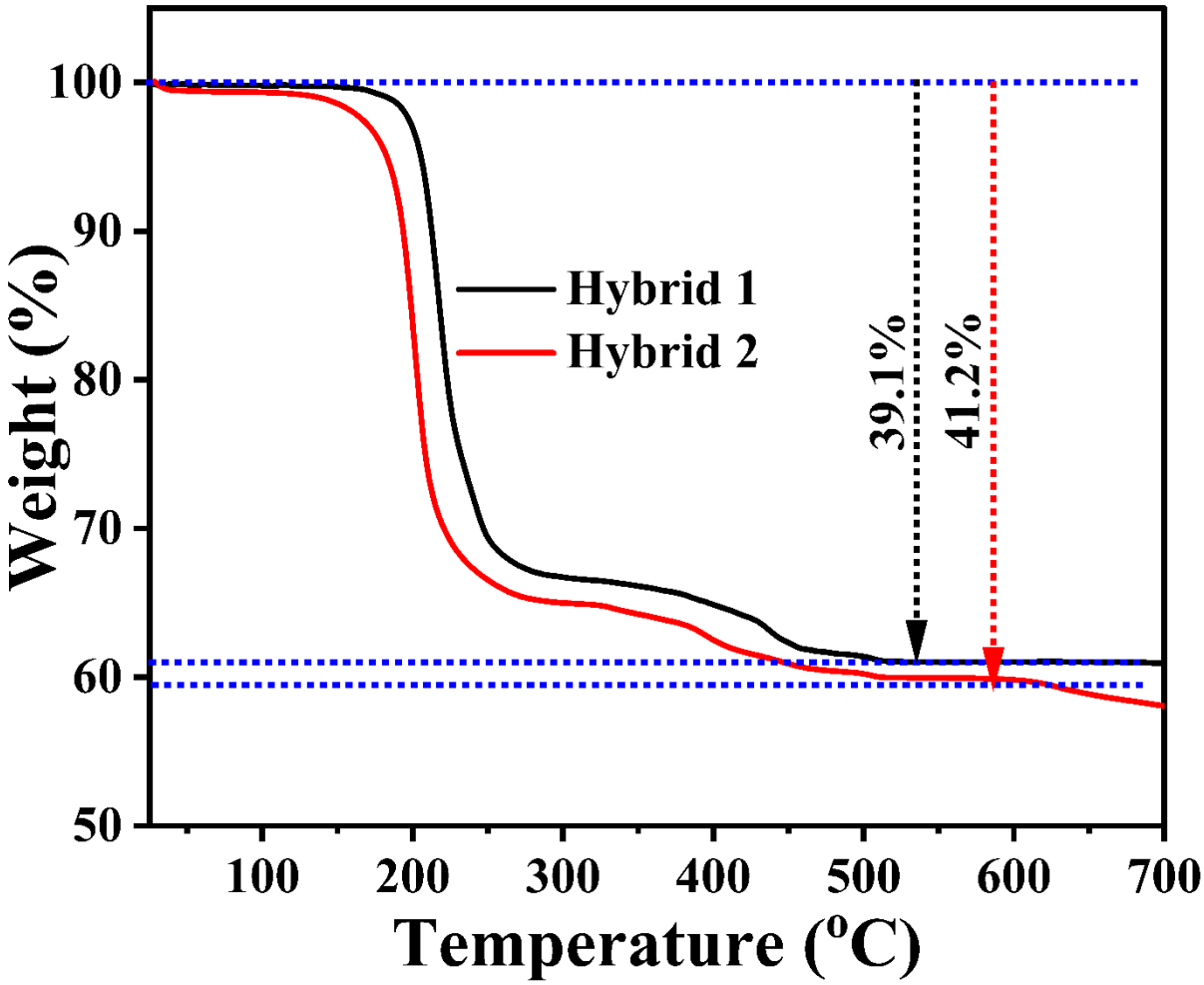

Fig. S8 TGA plots of hybrids **1** and **2**.

Table S3. Crystallographic data and structure refinement parameters of MDPSeT.

Empirical formula	$C_{14}H_{13}F_3O_3SSe$
Formula weight	394.731
Crystal system	monoclinic
Space group	$P2_1/c$
a/Å	12.6439(6)
b/Å	9.1730(4)
c/Å	15.4836(7)
α/°	90
β/°	112.955(6)
γ/°	90
V(Å^3)	1653.62(15)
Z	4
D_c (mg/mm^3)	1.586
F(000)	794.0
Reflections collected	4813 4813
Independent reflections	2997
Data/restraints/parameters	2997/0/200
GOF	1.044
Final R indexes [I>=2σ (I)]	R_1 = 0.0375, wR_2 = 0.0960
Final R indexes [all data]	R_1 = 0.0432, wR_2 = 0.1028

Table S4. Selected bond length (Å) and angles [°] for MDPSeT.

Se(1)-C(7)	1.924(3)	C(1)-C(2)	1.373(5)
Se(1)-C(13)	1.927(3)	C(1)-C(6)	1.367(5)
Se(1)-C(1)	1.923(3)	C(8)-C(9)	1.381(5)
S(1)-O(3)	1.424(2)	F(2)-C(14)	1.298(5)
S(1)-O(2)	1.441(3)	C(12)-C(11)	1.377(5)
S(1)-O(1)	1.431(2)	C(2)-C(3)	1.388(5)
S(1)-C(14)	1.804(4)	C(11)-C(10)	1.356(7)
C(7)-C(8)	1.385(4)	C(10)-C(9)	1.376(6)
C(7)-C(12)	1.369(4)	C(6)-C(5)	1.408(6)
F(1)-C(14)	1.324(5)	C(5)-C(4)	1.364(8)
F(3)-C(14)	1.313(5)	C(3)-C(4)	1.339(8)

C(13)-Se(1)-C(7)	101.41(12)	C(11)-C(12)-C(7)	118.7(3)
C(1)-Se(1)-C(7)	99.21(12)	C(3)-C2-C(1)	118.6(4)
C(1)-Se(1)-C(13)	102.60(14)	C(10)-C(11)-C(12)	120.8(4)
O(2)-S(1)-O(3)	113.15(17)	C(9)-C(10)-C(11)	120.4(3)
O(1)-S(1)-O(3)	115.07(16)	C(10)-C(9)-C(8)	120.3(4)
O(1)-S(1)-O(2)	115.13(17)	C(5)-C(6)-C(1)	118.1(4)
C(14)-S(1)-O(3)	103.6(2)	F(1)-C(14)-S(1)	111.0(3)
C(14)-S(1)-O(2)	103.8(2)	F(3)-C(14)-S(1)	111.5(3)
C(14)-S(1)-O(1)	104.2(2)	F(3)-C(14)-F(1)	105.8(4)
C(8)-C(7)-Se(1)	122.3(2)	F(2)-C(14)-S(1)	112.3(3)
C(12)-C(7)-Se(1)	115.9(2)	F(2)-C(14)-F(1)	108.0(5)
C(12)-C(7)-C(8)	121.7(3)	F(2)-C(14)-F(3)	108.0(4)
C(2)-C(1)-Se(1)	122.2(3)	C(4)-C(5)-C(6)	119.6(4)
C(6)-C(1)-Se(1)	116.0(3)	C(4)-C(3)-C(2)	120.6(5)
C(6)-C(1)-C(2)	121.8(3)	C(3)-C(4)-C(5)	121.3(4)
C(9)-C(8)-C(7)	118.1(3)		

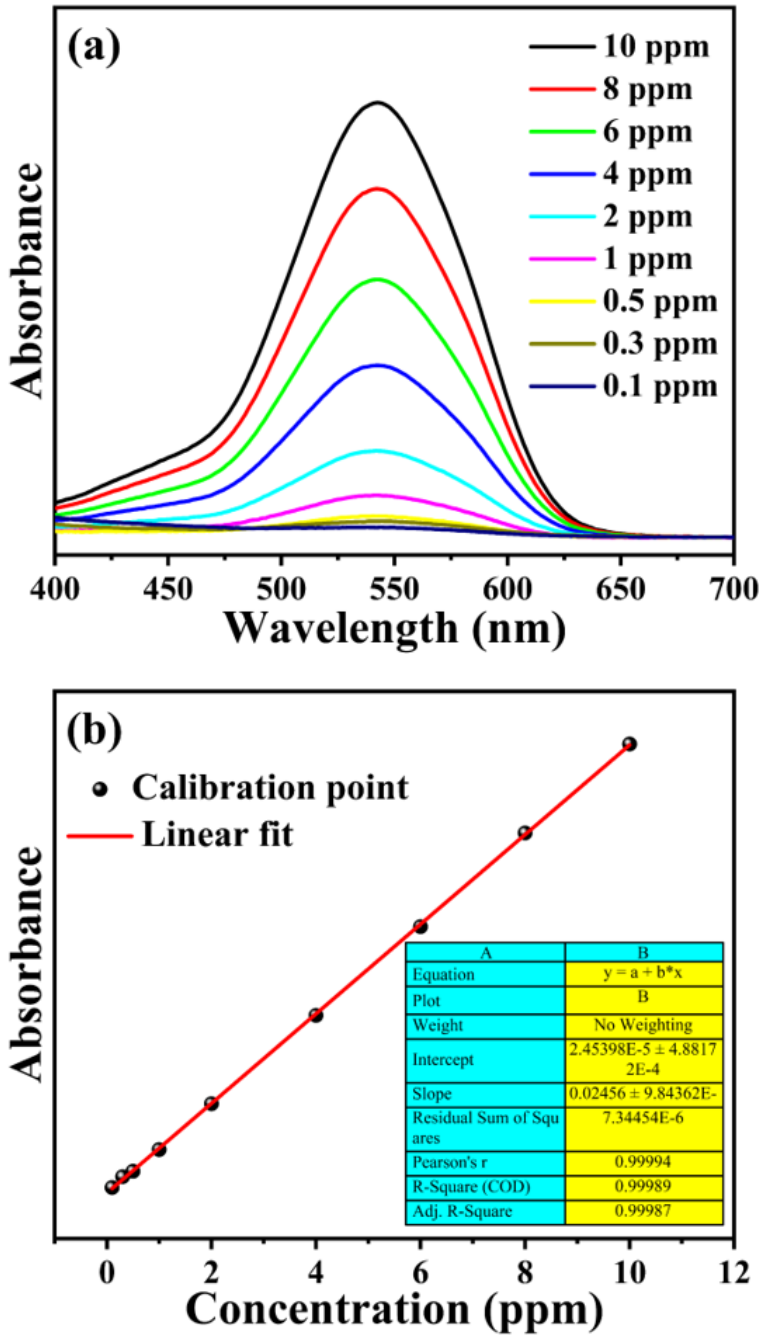

Fig. S9 (a) UV – Visible spectra recorded at various conc: for calibration plot; and (b) calibration point linear fit for different concentrations.

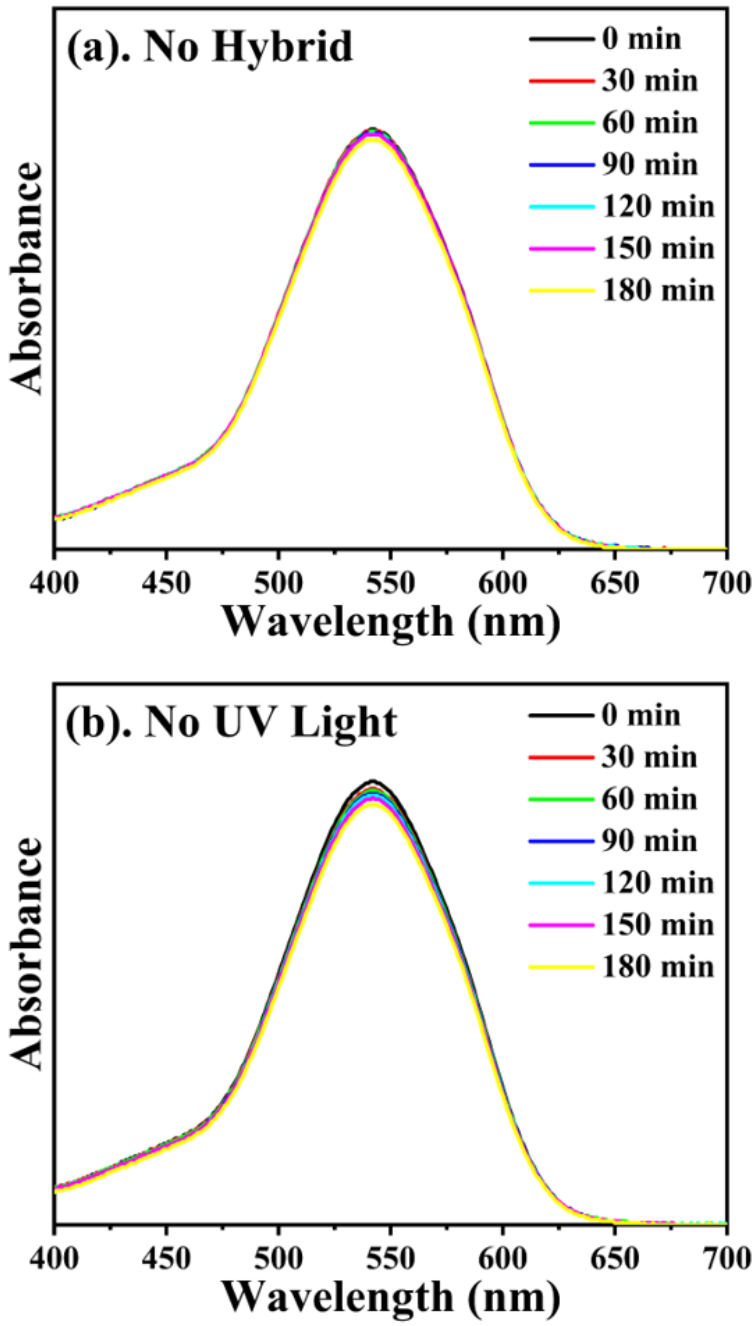

Fig. S10 The UV – vis spectra obtained from $[Cr_2O_7]^{2-}$ photoreduction control experiments: (a) without hybrid catalyst; and (b) without UV – irradiation.

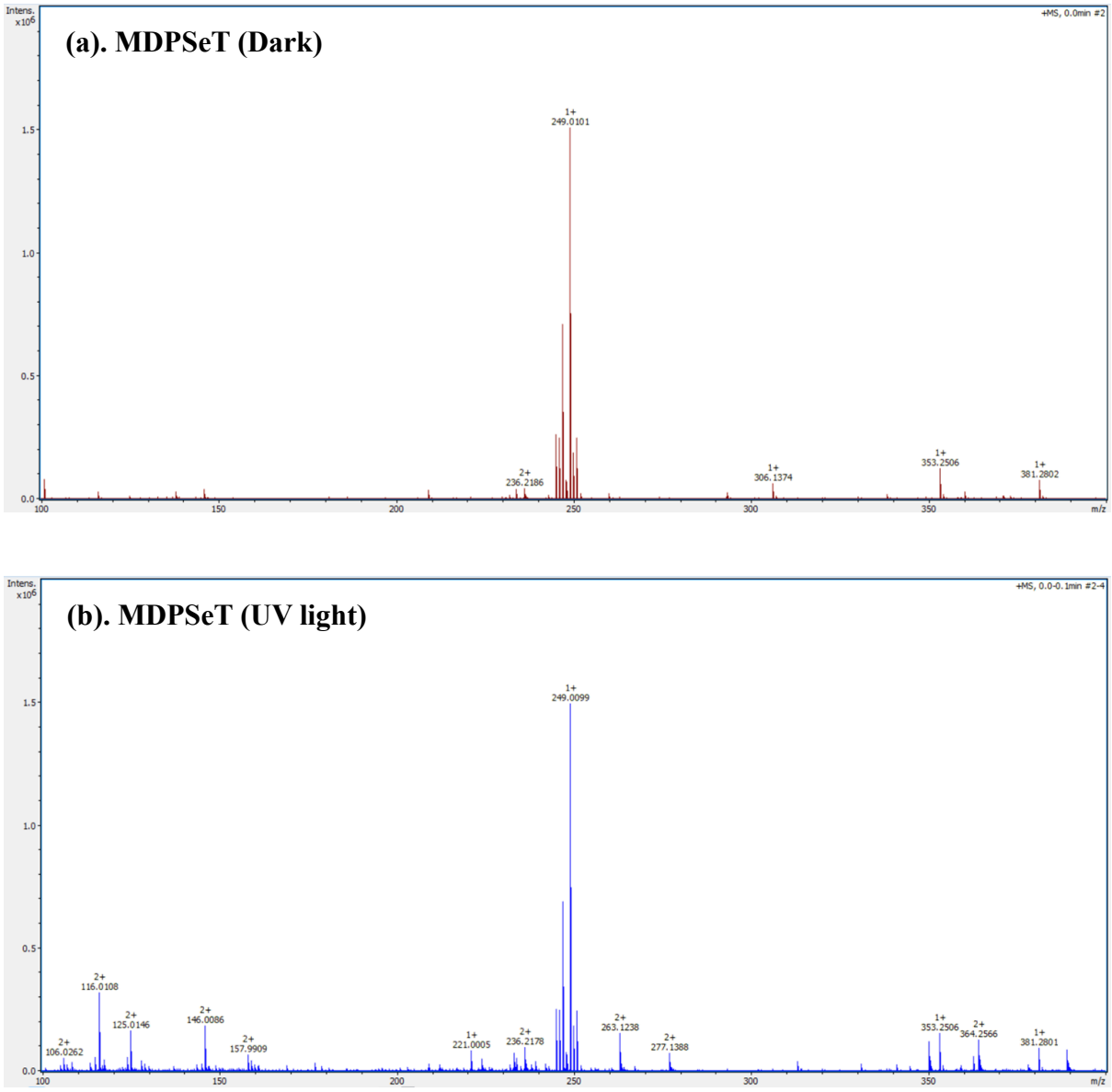

Fig. S11 ESI-MS (positive mode) data of MDPSeT after keeping for 3 h under (a) dark; and (b) UV irradiation.

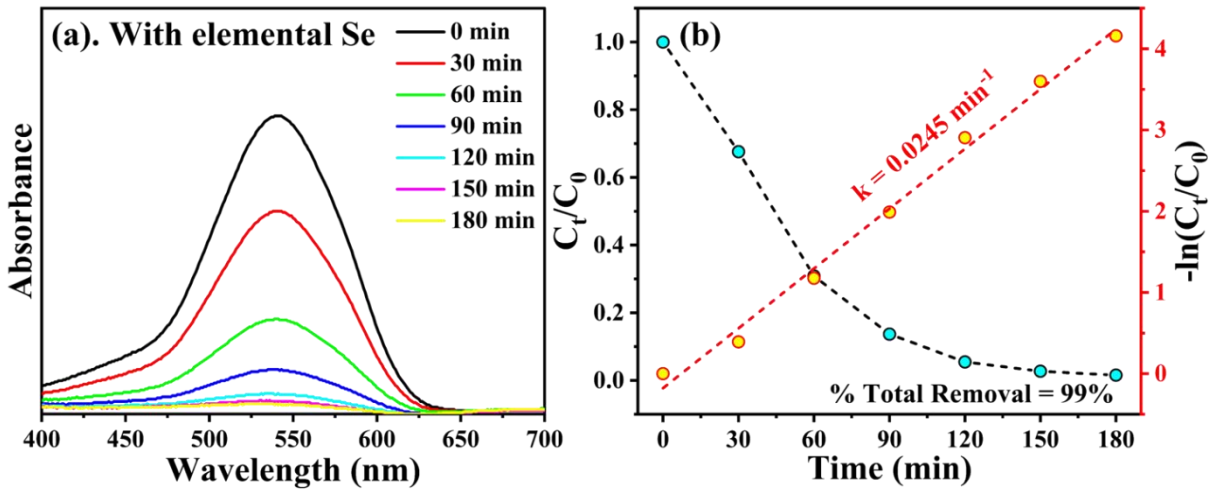

Fig. S12 (a) The UV – vis spectrum; and (b) kinetics study obtained from dichromate reduction using elemental selenium as catalyst.

Table S5. The comparison of photocatalytic activities of hybrid **2** with recently reported POM-photocatalysts toward Cr(VI) reduction.

Sr. No.	Photocatalyst	Cr(VI) conc. / volume	Total reduction/time	Light source	References
1.	FeSiW (4:3)	80 µmol/L – 50 mL	96%/90 min	Visible	4
2.	Hybrid **1**	3.8×10^{-4} M/7.5 mL	79%/20 min	Visible	5
3.	CN/PT-6	80 ppm/60 mL	82.77%/60 min	Visible	6
4.	$Co_6Zn_5W_{19}$	0.5 mmol L^{-1}/2.5 mL	Almost 100%/120 min	Visible	7
5.	Hybrid **5**	3.8×10^{-4} M/7.5 mL	92.83%/20 min	Visible	8
6.	Hybrid **2**	10 ppm/20 mL	99%/180 min	UV	This work

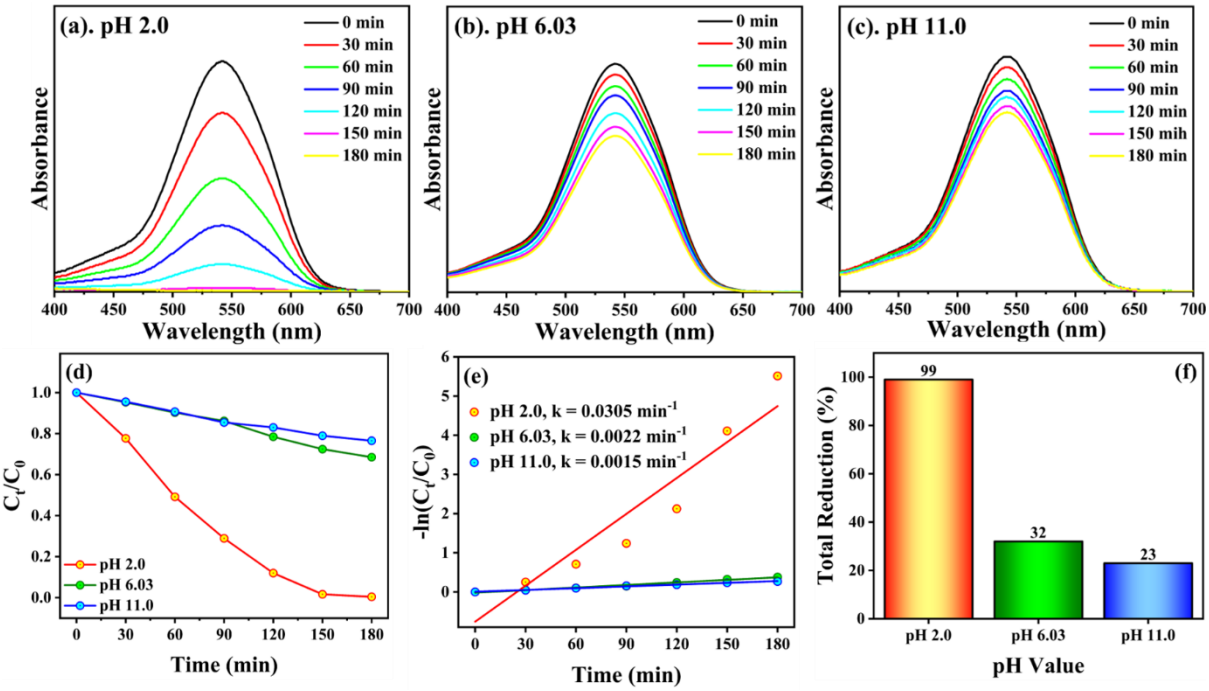

Fig. S13 (a-c) The UV – vis spectra obtained from $Cr_2O_7^{2-}$ photoreduction experiments; (d) concentration change; (e) rate constant; and (f) total photocatalytic reduction obtained under different pH conditions of the reaction medium.

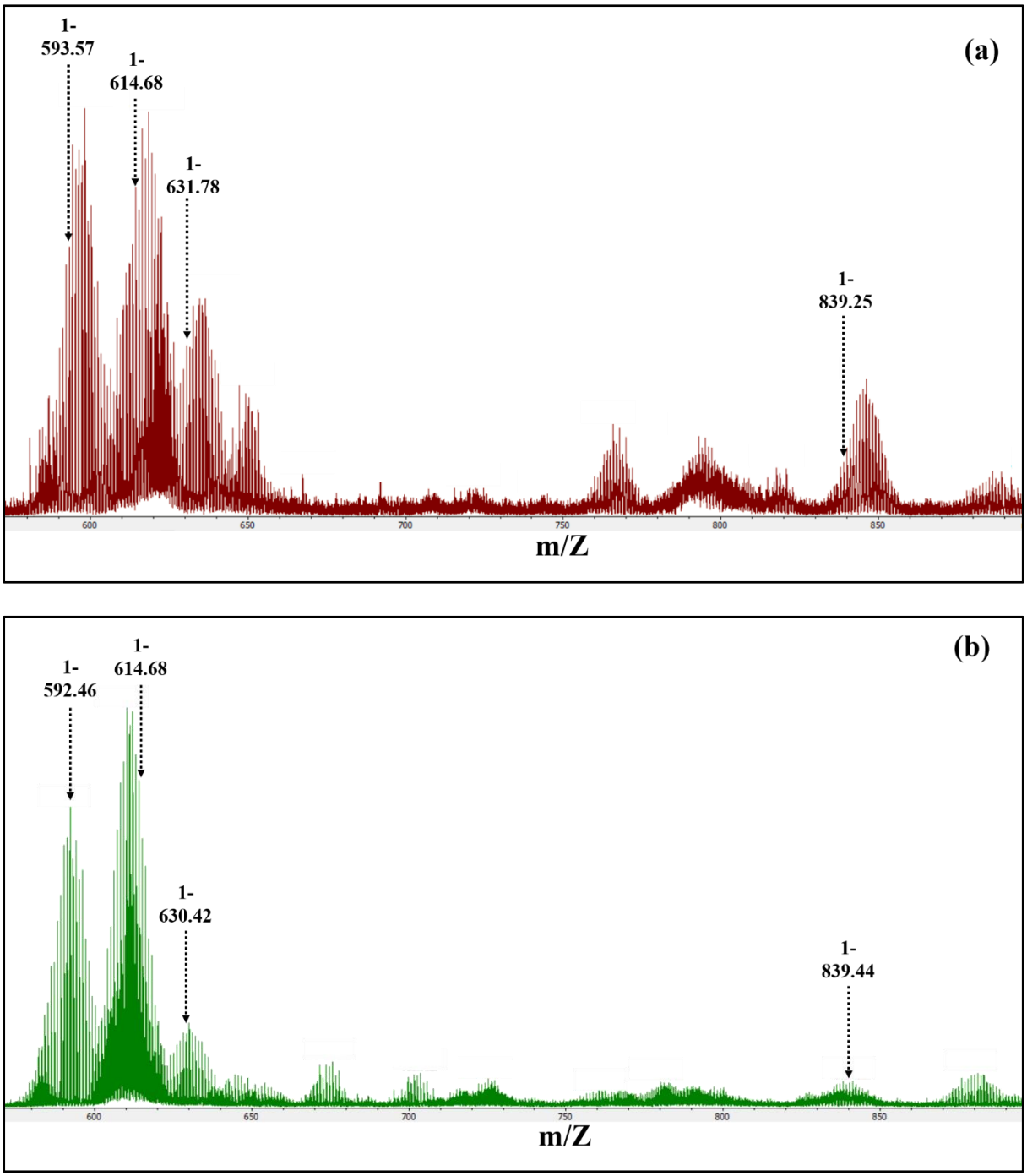

Fig. S14 ESI-MS data of (a) fresh hybrid **2**; and (b) after keeping for 18 h in solution a pH 2.

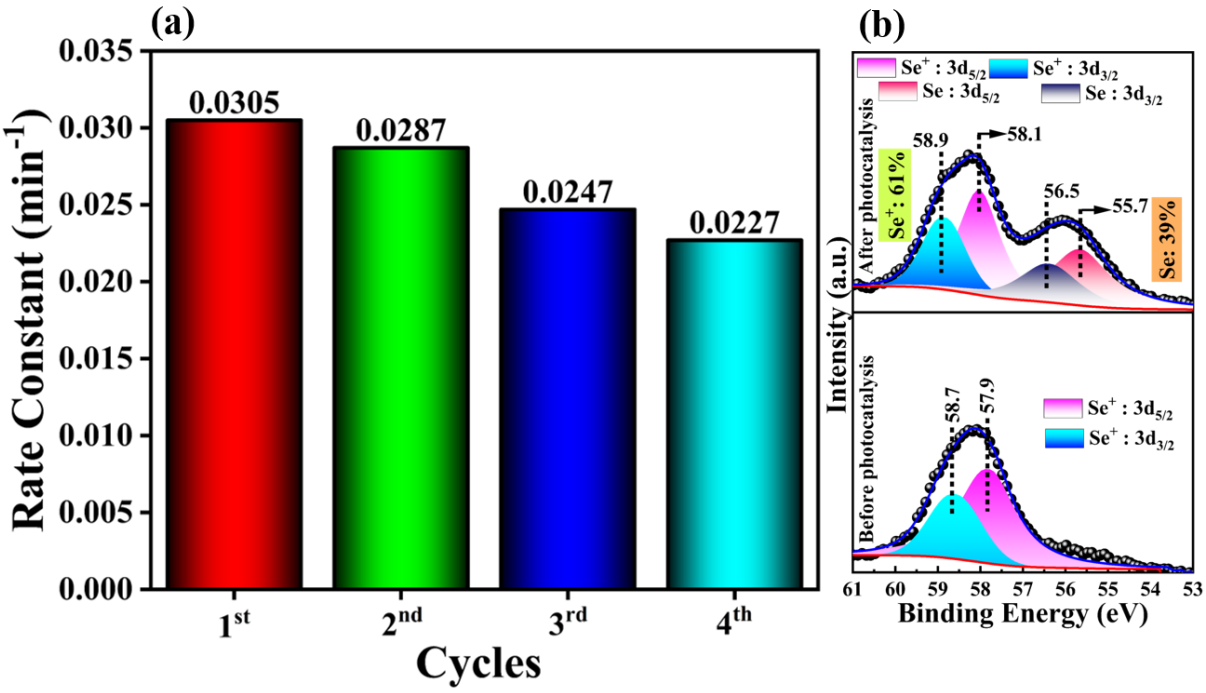

Fig. S15 (a) The rate constant values obtained for dichromate photocatalytic reduction in four different cycles; and (b) the XPS spectra of Se 3d confirming the two different oxidation states of selenium after dichromate photocatalytic reduction using hybrid **2**.

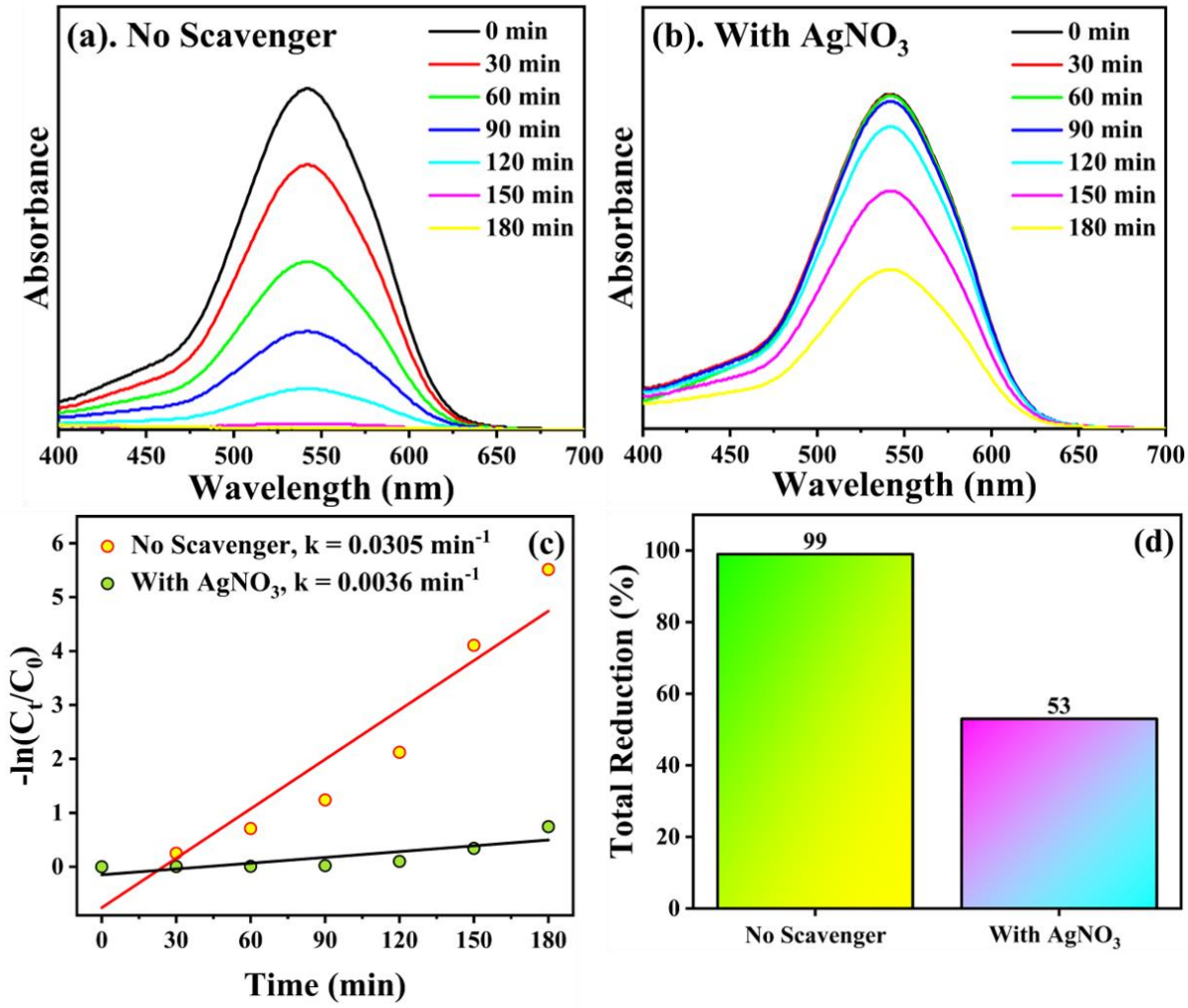

Fig. S16 The UV – vis spectra obtained from $[Cr_2O_7]^{2-}$ photoreduction scavenger study; (a) without; and (b) with scavenger. Comparison of the changes of (c) rate constant; and (d) total reduction with or without scavenger.

References

1. CrysAlisPro Program, version 171.37.33c, Agilent Technologies, *Oxford* **2012**.
2. G. M. Sheldrick, A short history of SHELX. *Acta Cryst.,* 2008, **A64**, 112-122.
3. O. V. Dolomanov, L. J. Bourhis, R. J. Gildea, J. A. K. Howard and H. Puschmann, OLEX2: a complete structure solution, refinement and analysis program. *J. Appl. Cryst.,* 2009, **42**(2), 339-341.
4. Q. Cen, Q. Gao, C. Zhang, Y. Liu, Q. Wang and Q. Wang, Photocatalytic reduction of Cr(VI) by iron tungstosilicate under visible light. *J. Colloid Interface Sci.,* 2020, **562**, 12-20.
5. Y.-Q. Zhang, L. Hou, H.-X. Bi, X.-X. Fang, Y.-Y. Ma and Z.-G. Han, Organic moiety-regulated photocatalytic performance of phosphomolybdate hybrids for hexavalent chromium reduction. *Chem. Asian J.,* 2021, **16**(12), 1584-1591.
6. H. Shi, T. Zhao, J. Wang, Y. Wang, Z. Chen, B. Liu, H. Ji, W. Wang, G. Zhang and Y. Li, Fabrication of g-C_3N_4/PW_{12}/TiO_2 composite with significantly enhanced photocatalytic performance under visible light. *J. Alloys Compd.,* 2021, **860**, 157924.
7. C. Si, P. Ma, Q. Han, J. Jiao, W. Du, J. Wu, M. Li and J. Niu, A Polyoxometalate-based Inorganic porous material with both proton and electron conductivity by light actuation: photocatalysis for Baeyer–Villiger oxidation and Cr(VI) reduction. *Inorg. Chem.,* 2020, **60**(2), 682-691.
8. H.-X. Bi, L. Hou, X.-Y. Yin, Y.-Y. Ma and Z.-G. Han, Central metals to guide the bandgap of hourglass-type polyoxometalate hybrids as photocatalyst for the reduction of Cr(VI). *Cryst. Growth Des.,* 2022, **22**(1), 738-746.